Published on 04 March 2013. Downloaded by Hefei Institutes of Physical Science, Chinese Academy of Sciences on 02/09/2013 02:46:12.

CrystEngComm

RSC Publishing

COMMUNICATION

View Article Online
View Journal | View Issue

Influence of Sb doping on the structural and optical properties of tin oxide nanocrystals†

Cite this: *CrystEngComm*, 2013, **15**, 3296

Received 5th February 2013,
Accepted 1st March 2013

DOI: 10.1039/c3ce40241j

www.rsc.org/crystengcomm

J. M. Xu, L. Li, S. Wang, H. L. Ding, Y. X. Zhang and G. H. Li

The influence of Sb doping on the structural and optical properties of the SnO_2 nanocrystals and films were investigated. An unusual enhancement in near infrared absorption was found in the SnO_2 nanocrystals with increasing Sb doping content, and the maximum absorption shifted to shorter wavelength.

Tin oxide is an important n-type semiconductor with a large band gap (E_g = 3.6 eV, at 300 K). As one of the most promising functional semiconductor materials, SnO_2 has stimulated considerable research interest for its wide application in various fields such as gas sensors,[1,2] Li ion batteries,[3,4] solar cells[5] and photocatalysis.[6] Doping with an appropriate element, such as In, Nb, Ta and Sb, can modulate the optical and electrical properties of SnO_2,[7] in which the Sb is the most common dopant in SnO_2.

Antimony doped tin oxide (ATO) is an important transparent conductive oxide (TCO) with high visible transmission, excellent electrical properties and good stability. Previous studies were mainly focused on the ATO thin films fabricated by methods such as magnetron sputtering,[8] spray pyrolysis[9] and chemical vapor deposition.[10] Recently, the synthesis of ATO nanoparticles has aroused great interest due to their potential applications in Li ion batteries,[11] gas sensors,[12] electrochromic windows,[13] transparent electrodes[14] and heat-insulating films.[15,16] Different methods have been explored to synthesize ATO nanoparticles including coprecipitation,[17] combustion[18] and sol–gel routes.[19] The ATO nanoparticles with uniform size distribution and good dispersity have achieved by hydrothermal or solvothermal methods.[20] Nanosized monodispersed ATO nanocrystals have been obtained by a nonaqueous sol–gel procedure.[21] The ATO nanocrystals doped with 18 mol% Sb have been prepared by using "benzyl alcohol route".[22]

Key Laboratory of Materials Physics, Anhui Key Laboratory of Nanomaterials and Nanotechnology, Institute of Solid State Physics, Chinese Academy of Sciences, Hefei 230031, P. R. China. E-mail: ghli@issp.ac.cn

† Electronic supplementary information (ESI) available: Fig. S1, particle size distribution diagrams of Sb doped SnO_2 nanocrystals. Fig. S2, XPS spectra of Sb doped SnO_2 nanocrystals. Fig. S3, FESEM images of 10% ATO nanocrystals film. See DOI: 10.1039/c3ce40241j

The visible transmission and near infrared (NIR) block properties of ATO thin films depend strongly on the Sb doping content.[23,24] An ATO nanocrystal film with a limited size and good dispersion can maintain high visible transparency due to the decrease in the scattering of light,[20] and a relative low reflection in the NIR region in comparison to the films deposited by traditional physical and chemical vapor deposition.[25] Nevertheless, the underline mechanisms of those behaviors of ATO nanocrystals film is still not very clear.

In this communication, we report the solvothermal synthesis of Sb doped SnO_2 nanocrystals by using benzyl alcohol as solvent. We found that the size of SnO_2 nanocrystals gradually decreases while NIR absorption remarkably increases with increasing Sb doping content. The NIR block behavior of the ATO nanocrystal film results from the enhanced absorption due to the increased free electron concentration.

XRD analyses (Fig. 1) indicate that all the diffraction peaks of the as-prepared samples can be well indexed into tetragonal rutile SnO_2 (JCPDS card No 88-0287) without any indication of other phases, such as Sb_2O_3 or Sb_2O_5, implying that the Sb doping occurs by substituting Sn atoms in the SnO_2 crystal structure. The average crystallite size as estimated by Scherrer equation ($d = 0.89\lambda/(B\cos\theta)$, where d, λ, B and θ are the grain size, X-ray wavelength, the full-width-at-half-maximum and Bragg angle, respectively) is about 11.4, 10.5, 9.6 and 8.8 nm for SnO_2 nanoparticles doped with 0, 2, 6 and 10% Sb, respectively.

TEM observations reveal that small spherical and large quadrate nanoparticles coexist in the undoped SnO_2 sample with average size of about 11.3 nm (Fig. 2a). With increasing Sb doping content, the average size of SnO_2 nanoparticles gradually decreases, and has an average size of about 10.7, 9.8 and 8.5 nm with Sb doping content of 2, 6 and 10% (Fig. 2c–e), respectively (size distribution is shown in Fig. S1, ESI†), which are in good agreement with the XRD results. HRTEM observations further proved that the ATO nanoparticles are single crystalline (Fig. 2e), the clear lattice fringes with spacings of about 0.335 nm correspond to the (110) interplanar distances of rutile SnO_2. The obvious color change can be observed from the digital images of the Sb-doped SnO_2 nanocrystals dispersed in cyclohexane solution

This journal is © The Royal Society of Chemistry 2013

Published on 04 March 2013. Downloaded by Hefei Institutes of Physical Science, Chinese Academy of Sciences on 02/09/2013 02:46:12.

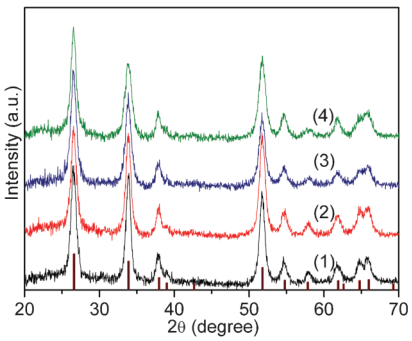

Fig. 1 XRD patterns of SnO_2 nanoparticles with Sb doping content of (1) 0, (2) 2, (3) 6 and (4) 10%.

(Fig. 2f), which is an indication of the presence of electrons in the conduction band due to Sb doping.[26,27]

The XPS analysis demonstrates the existence of only Sn, Sb and O without any impurities in the Sb-doped SnO_2 nanocrystals (Fig. S2a, ESI†). The binding energies at 486.5 and 495.0 eV are attributed to Sn $3d_{5/2}$ and Sn $3d_{3/2}$, respectively (Fig. S2b, ESI†), which are in a good agreement with the reported values in literature.[28] The XPS peak for Sb $3d_{3/2}$ shows a slight hump on the low energy side (Fig. S2c, ESI†) and the corresponding Gaussian fitting gives two binding energies at 539.1 and 540.2 eV and can be respectively assigned to Sb^{3+} $3d_{3/2}$ and Sb^{5+} $3d_{3/2}$ in the tin oxide lattice. The coexistence of the oxidation states of Sb^{3+} and Sb^{5+} has been constantly observed in ATO materials.[12,29] The Sb^{5+} ions substitute for Sn^{4+} ions forming a shallow donor level close to the

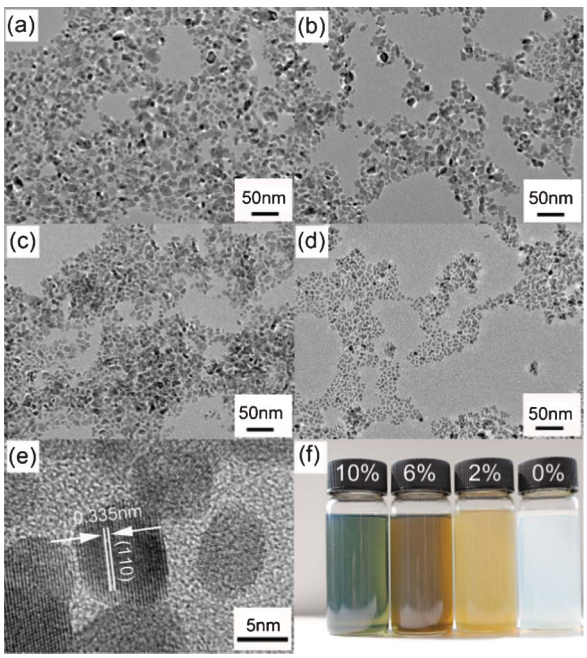

Fig. 2 TEM images of SnO_2 nanoparticles with Sb doping content of (1) 0, (2) 2, (3) 6 and (4) 10%. (e) HRTEM image of the nanoparticles in (d). (f) Digital images of SnO_2 nanoparticles doped with different contents of Sb dispersed in cyclohexane solution.

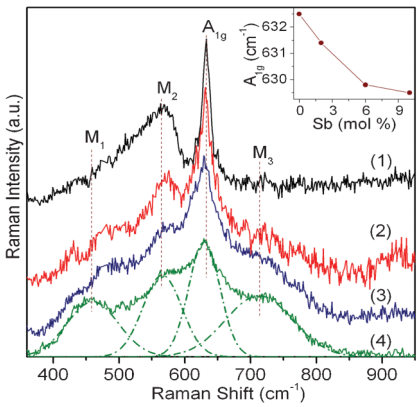

Fig. 3 Raman spectra of SnO_2 nanocrystals with Sb doping content of (1) 0, (2) 2, (3) 6 and (4) 10%. The inset shows dependence of peak position of A_{1g} vibration on the Sb doping content.

conduction band of SnO_2, while the Sb^{3+} ion doping introduces a shallow acceptor level close to the valence band. The free carrier concentration directly depends on the ratio of Sb^{5+} and Sb^{3+} sites. The results shown in Fig. S1c, ESI,† proved that the ATO nanocrystals doped with different Sb contents all contain Sb^{5+} and Sb^{3+} ions. The fact that the peak area of Sb^{5+} is larger than that of Sb^{3+} indicates that the effective donor concentration is higher than acceptor concentration, and thus the ATO nanocrystals prepared in the present study have a high free electrons concentration. The actual doping contents obtained by the quantitative calculation from high solution scans of Sb $3d_{3/2}$ and Sn $3d_{3/2}$ were found to be about 1.8, 5.7 and 9.1 at%, which are slightly lower than the target contents.

Fig. 3 shows the room temperature Raman spectra of as-prepared SnO_2 nanocrystals doped with different Sb contents. The Raman peak at about 632.7 cm^{-1} for SnO_2 nanocrystals can be assigned to A_{1g} mode,[30] corresponding to the vibration perpendicular to the *c*-axis and slightly shifts to lower frequency with increasing Sb doping content (the inset in Fig. 3). This shift is due to the replacement of Sn ions by Sb ions within the SnO_2 lattice.[31] Three broad Raman peaks at 458, 566 and 720 cm^{-1} are assigned to surface vibration modes of SnO_2 nanocrystals, which generally can not be observed in bulk SnO_2.[30] It is well known that some inactive vibration modes in bulk material can be active owing to the size effect in very small particles or in nanostructures with some reduced dimension.[32,33] The intensity of these bands changes with increasing antimony content, which can be correlated to vibration modes of incorporated Sb ions inside the SnO_2 lattice.[21]

The UV-Vis-NIR absorption spectra of the oleylamine modified SnO_2 nanocrystals doped with different Sb contents in perchloroethylene solution reveal that there is only one absorption band in the near UV range for the SnO_2 nanocrystals (see curve (1) in Fig. 4), resulting from the band gap absorption of SnO_2 nanocrystals.[34] Meanwhile, for ATO nanocrystals, except for the strong band gap absorption, the Sb doping results in the absorbance in the NIR range.[26] The NIR absorption of the 2% and 6% ATO nanocrystals increased monotonically with wave-

Published on 04 March 2013. Downloaded by Hefei Institutes of Physical Science, Chinese Academy of Sciences on 02/09/2013 02:46:12.

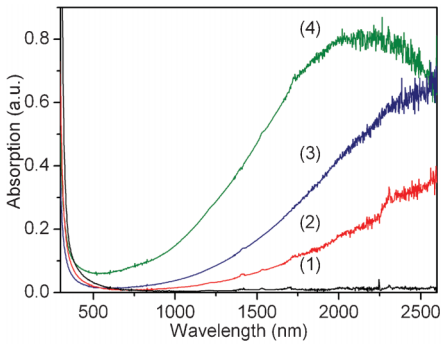

Fig. 4 UV-Vis-NIR absorption of oleylamine modified SnO_2 nanocrystals with Sb doping content of (1) 0, (2) 2, (3) 6 and (4) 10% dispersed in perchloroethylene solution.

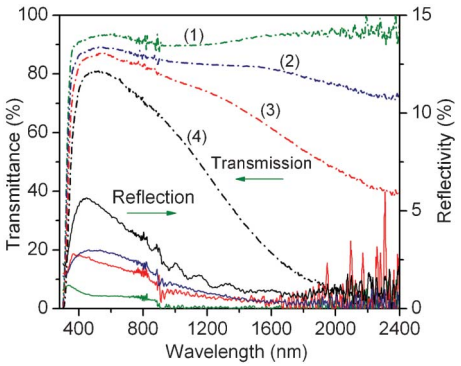

Fig. 5 Transmission and reflection spectra of SnO_2 nanocrystals films with Sb doping content of (1) 0, (2) 2, (3) 6 and (4) 10%.

length without reaching a maximum, as shown in curves (2) and (3) of Fig. 4, respectively, which is a typical absorption feature of doped semiconductor while for 10% ATO there is a distinct broad NIR absorption peak with maximum at about 2200 nm, as shown in curve (4) of Fig. 4. The appearance of absorption in the infrared region is a clear signature of n-type doping[35–37] and can be attributed to surface plasmon absorption in ATO.[13] According to the Drude model the absorption coefficient, α, associated with the free electron in n-type semiconductors, is directly proportional to the charge carrier density, N, from the following equation:[38]

$$\alpha = \frac{Ne^2}{m_e \varepsilon_0 n c \tau \omega^2} \quad (1)$$

where e is the electron charge, m_e the effective mass of an electron, ε_0 the vacuum permittivity, τ the relaxation time of free electrons, n the refractive index of undoped semiconductor, and c and ω the speed and frequency of light, respectively. In addition, the infrared absorption position of the plasmon band is directly proportional to the electron plasma frequency, ω_p, according to following expression:[38]

$$\omega_{sp}{}^2 = \frac{\omega_p{}^2}{1+\varepsilon_m} \quad (2)$$

where ω_{sp} is the surface plasma absorption frequency, ε_m is dielectric constant of the surrounding medium and ω_p is known as the electron plasma frequency, which has a square root dependence on the free electron concentration:[38]

$$\omega_p = \sqrt{\frac{Ne^2}{m_e \varepsilon_\infty \varepsilon_0}} \quad (3)$$

where ε_∞ is the optical dielectric constant. From above equations one can see that the strong near infrared absorption of n-typed semiconductor nanocrystals originate from free electron absorption in the near infrared region and the surface plasma absorption position can be tuned by variation of free electron concentration. The increase in free electron concentration with increasing Sb content will thus lead to the enhanced NIR absorption and the blue shift of the maxima.

FESEM observations reveal that Sb-doped SnO_2 nanocrystals films are uniform and consists of many nanocrystals (Fig. S3, ESI†). From the corresponding transmission and reflection spectra (Fig. 5), one can see that the transmittance of the pure SnO_2 nanocrystals film can reach as high as 90% in visible light region, while that of the ATO nanocrystal films gradually decreases with increasing Sb content due to the direct photon absorption and the increased photon scattering, but still all exceeds 80%. It is worth noting that the reflection in the visible light region slightly increases with increasing Sb doping content while that in NIR region is nearly zero. Similar results have been observed in other TCO nanocrystal films.[25,39] The excellent NIR block is considered to result from the strong NIR absorption of free electrons. The infrared reflection R can be given by:[40,41]

$$R = 1 - \frac{2}{\omega_p \varepsilon_\infty{}^{1/2} \tau} \quad (4)$$

From eqn (1) and (4), one can see that the reflection and absorption depends strongly on the relaxation time of free electrons, the shorter the relaxation time, the higher the absorption and the lower the reflection. Due to the small crystal size and loose structure, the relaxation time of free electrons in ATO nanocrystal films is relative low, and thus results in a low reflection and strong absorption in the NIR region.

In summary, we have synthesized SnO_2 nanocrystals with different Sb doping content by a facile one-step solvothermal method. The crystal size decreases, the A_{1g} mode vibration shows a red shift with increasing Sb content in the ATO nanocrystals. The Sb^{3+} and Sb^{5+} can coexist in the ATO nanocrystals and the effective concentration of donor Sb^{5+} is higher than that of the acceptor Sb^{3+}. The NIR absorption of ATO nanocrystals enhances with the increase of Sb content with the maximum band shifting to shorter wavelength due to the increased free electron concentration. The ATO nanocrystals film has a high visible light transmittance and nearly zero NIR reflection. Our results demonstrate that the ATO nanocrystal films have excellent optical properties with promise as a heat insulation coating in the energy conservation field and transparent electrodes in the optoelectronic field.

 This journal is © The Royal Society of Chemistry 2013

Published on 04 March 2013. Downloaded by Hefei Institutes of Physical Science, Chinese Academy of Sciences on 02/09/2013 02:46:12.

Experimental

Chemicals

Tin(IV) tetrachloride, oleylamine and oleic acid were purchased from Aladdin, antimony(III) trichloride, benzyl alcohol, perchloroethylene, acetone, ethanol and cyclohexane were purchased from Sinopharm Chemical Reagent Co., Ltd. and were of analytical reagent grade and used without further purification.

Preparation of Sb-doped SnO_2 nanocrystals

In a typical preparation of 10 at% ATO, 2.7 mmol $SnCl_4$ and 0.3 mmol $SbCl_3$ were dissolved in 50 ml benzyl alcohol in a closed glass vessel, and then the mixture was stirred with a magnetic stirrer for 1 h before being transferred to a Teflon-lined autoclave. The autoclave was kept at 200 °C for 24 h and then cooled to room temperature naturally. The nanocrystals were separated by centrifugation at 7000 rcf for 10 min, and then washed three times with acetone. The target Sb doping content is 2, 6 and 10 at%. To prepare the nanocrystal dispersions, 0.1 g nanocrystals were dispersed in 20 ml cyclohexane with the addition of a few drops of oleylamine.

Preparation of Sb-doped SnO_2 nanocrystals films

Firstly, a glass substrate was treated at 80 °C with oleic acid, in which the substrate will change to hydrophobic from hydrophilic due to the formation of a very thin oleic acid layer on its surface. Then, the nanocrystal dispersion was spin-coated onto the functionalized substrate. The thickness of the nanocrystal film is controlled *via* changing the spinning rate and coating times. Finally, the films were annealed in air at 550 °C for 1 h to remove the organic contaminants.

X-ray diffraction (XRD) analyses were carried out on Philips X'Pert using Cu Kα line. The morphology and microstructure were examined using field emission scanning electron microscopy (FESEM, Sirion 200) and transmission electron microscopy (TEM, JEOL-2010). X-ray photoelectron spectrum (XPS) was recorded on a VG ESCALAB Mark II X-ray photoelectron spectroscope. Raman spectra were measured at room temperature using a confocal microprobe Raman system (Renishaw, inVia) with the excitation wavelength of 532 nm. The UV-Vis-NIR spectra were recorded on a Shimadzu UV3600 spectrophotometer.

Acknowledgements

This work was financially supported by the National Basic Research Program of China (2009CB939903), and innovation project of the Chinese Academy of Sciences (KJCX2-YW-H2O).

References

1 H. J. Zhang, Q. Q. He, X. D. Zhu, D. Y. Pan, X. Y. Deng and Z. Jiao, *CrystEngComm*, 2012, **14**, 3169–3176.
2 A. Sharma, M. Tomar and V. Gupta, *J. Mater. Chem.*, 2012, **22**, 23608–23616.
3 C. H. Xu, J. Sun and L. Gao, *J. Mater. Chem.*, 2012, **22**, 975–979.
4 J. S. Chen, M. F. Ng, H. B. Wu, L. Zhang and X. W. Lou, *CrystEngComm*, 2012, **14**, 5133–5136.
5 Z. D. Li, Y. Zhou, T. Yu, J. G. Liu and Z. G. Zou, *CrystEngComm*, 2012, **14**, 6462–6468.
6 S. S. Wu, H. Q. Cao, S. F. Yin, X. W. Liu and X. R. Zhang, *J. Phys. Chem. C*, 2009, **113**, 17893–17898.
7 Y. D. Wang, T. Brezesinski, M. Antonietti and B. Smarsly, *ACS Nano*, 2009, **3**, 1373–1378.
8 J. Montero, C. Guillen and J. Herrero, *Sol. Energy Mater. Sol. Cells*, 2011, **95**, 2113–2119.
9 S. Y. Lee and B. O. Park, *Thin Solid Films*, 2006, **510**, 154–158.
10 R. Outemzabet, N. Bouras and N. Kesri, *Thin Solid Films*, 2007, **515**, 6518–6520.
11 Y. D. Wang, I. Djerdj, B. Smarsly and M. Antonietti, *Chem. Mater.*, 2009, **21**, 3202–3209.
12 J. M. Wu, *Nanotechnology*, 2010, **21**, 235501.
13 U. Zum Felde, M. Haase and H. Weller, *J. Phys. Chem. B*, 2000, **104**, 9388–9395.
14 J. Lim, B. Y. Jeong, H. G. Yoon, S. N. Lee and J. Kim, *J. Nanosci. Nanotechnol.*, 2012, **12**, 1675–1678.
15 J. Feng, B. Y. Huang and M. Q. Zhong, *J. Colloid Interface Sci.*, 2009, **336**, 268–272.
16 Y. Shieh, P. C. Hsieh and C. J. Chen, *Adv. Mater. Res.*, 2011, **168–170**, 1670–1674.
17 D. W. Kim, D. S. Kim, Y. G. Kim, Y. C. Kim and S. G. Oh, *Mater. Chem. Phys.*, 2006, **97**, 452–457.
18 Y. Q. Li, J. L. Wang, S. Y. Fu, S. G. Mei, J. M. Zhang and K. Yong, *Mater. Res. Bull.*, 2010, **45**, 677–681.
19 T. G. Conti, A. J. Chiquito, R. O. Da Silva, E. Longo and E. R. Leite, *J. Am. Ceram. Soc.*, 2010, **93**, 3862–3866.
20 L. L. Li, L. M. Mao and X. C. Duan, *Mater. Res. Bull.*, 2006, **41**, 541–546.
21 V. Muller, M. Rasp, G. Stefanic, J. H. Ba, S. Gunther, J. Rathousky, M. Niederberger and D. Fattakhova-Rohlfing, *Chem. Mater.*, 2009, **21**, 5229–5236.
22 R. O. da Silva, T. G. Conti, A. F. de Moura, D. G. Stroppa, L. C. G. Freitas, C. Ribeiro, E. R. Camargo, E. Longo and E. R. Leite, *ChemPhysChem*, 2009, **10**, 841–846.
23 C. Terrier, J. P. Chatelon and J. A. Roger, *Thin Solid Films*, 1997, **295**, 95–100.
24 A. R. Babar, S. S. Shinde, A. V. Moholkar, C. H. Bhosale, J. H. Kim and K. Y. Rajpure, *J. Alloys Compd.*, 2010, **505**, 416–422.
25 T. Izumi, K. Izumi, N. Kuroiwa, A. Senjuh, A. Fujimoto, M. Adachi and T. Yamamoto, *J. Alloys Compd.*, 2009, **480**, 123–125.
26 T. Nutz, U. zum Felde and M. Haase, *J. Chem. Phys.*, 1999, **110**, 12142–12150.
27 T. Nutz and M. Haase, *J. Phys. Chem. B*, 2000, **104**, 8430–8437.
28 Y. Wang, T. Brezesinski, M. Antonietti and B. Smarsly, *ACS Nano*, 2009, **3**, 1373–1378.
29 Y. Wang, Q. Mu, G. Wang and Z. Zhou, *Sens. Actuators B*, 2010, **145**, 847–853.
30 J. F. Scott, *J. Chem. Phys.*, 1970, **53**, 852–853.
31 F. H. Aragon, J. A. H. Coaquira, P. Hidalgo, S. W. da Silva, S. L. M. Brito, D. Gouvea and P. C. Moraisa, *J. Raman Spectrosc.*, 2011, **42**, 1081–1086.
32 L. Z. Liu, T. H. Li, X. L. Wu, J. C. Shen and P. K. Chu, *J. Raman Spectrosc.*, 2012, **43**, 1423–1426.
33 M. N. Rumyantseva, A. M. Gaskov, N. Rosman, T. Pagnier and J. R. Morante, *Chem. Mater.*, 2005, **17**, 893–901.
34 T. Nütz and M. Haase, *J. Phys. Chem. B*, 2000, **104**, 8430–8437.
35 M. Kanehara, H. Koike, T. Yoshinaga and T. Teranishi, *J. Am. Chem. Soc.*, 2009, **131**, 17736–17737.

Published on 04 March 2013. Downloaded by Hefei Institutes of Physical Science, Chinese Academy of Sciences on 02/09/2013 02:46:12.

36 K. Manthiram and A. P. Alivisatos, *J. Am. Chem. Soc.*, 2012, **134**, 3995–3998.
37 Q. Q. Huang, S. Hu, J. Zhuang and X. Wang, *Chem.–Eur. J.*, 2012, **18**, 15283–15287.
38 A. M. Fox, *Optical Properties of Solids*, Oxford Univ Pr, 2010.
39 J. Ederth, P. Johnsson, G. A. Niklasson, A. Hoel, A. Hultaker, P. Heszler, C. G. Granqvist, A. R. van Doorn, M. J. Jongerius and D. Burgard, *Phys. Rev. B: Condens. Matter Mater. Phys.*, 2003, **68**, 155410.
40 A. Solieman and M. A. Aegerter, *Thin Solid Films*, 2006, **502**, 205–211.
41 J. Ederth, G. A. Niklasson, A. Hultaker, P. Heszler, C. G. Granqvist, A. R. van Doorn, M. J. Jongerius and D. Burgard, *J. Appl. Phys.*, 2003, **93**, 984–988.

 This journal is © The Royal Society of Chemistry 2013